

Hydrodynamic forces on particles considering realistic morphologies

Kushal Manjunath¹, N.S.S.P Kalyan¹, Ramesh Kannan Kandasami^{1,*}, and Subhadeep Banerjee¹

¹Department of Civil Engineering, Indian Institute of Technology Madras, Chennai – 600036

Abstract. The study investigates the complex relationship between particle morphology and hydrodynamic behavior through CFD simulations using OpenFOAM’s simpleFoam solver. Three distinct particle shapes—elongated, rounded, and angular were analyzed in the laminar regime. A comprehensive morphological characterization was performed using various descriptors to identify the most influential parameter governing flow behavior. The pressure and viscous drag components in the X, Y, and Z directions were quantified for flows parallel to the major and minor particle axes. The results demonstrate a significant dependence of morphology on hydrodynamic forces and flow characteristics. A clear trend of drag force components with the morphology indices was observed. Elongated particles exhibited the most pronounced orientation-dependent behavior. However, particles with a higher Corey shape factor had the most consistent behavior across different flow directions.

1 Introduction

The hydrodynamic behavior of rock particles/ aggregates in fluid environments has numerous applications in sediment transport and debris flow analysis [1]. This study comprehensively investigates the relationship between particle shape characteristics and hydrodynamic response by examining the particles’ realistic morphologies and surficial features using the X-ray CT scanned images. Morphology is quantified through descriptors that provide a mathematical framework for characterizing their interaction with the surrounding fluid, affecting the pressure and viscous drag coefficients. Flow is oriented parallel to both major and minor particle axes to observe orientation-dependent behaviors. Both the viscous and pressure components are studied. It is well known that the hydrodynamic response changes with the Reynolds number. However, in this study, only the laminar regime is adopted.

2 Numerical model

To study the hydrodynamic behavior of individual particles, the fluid domain is set up as shown in Figure 1a, 1b. The particle walls or surface are set as the no-slip condition. The outlet pressure is set to 0 Pa, and the surrounding walls have periodic boundary conditions to minimize wall effects. The particle centroid is placed at a distance of ‘5d_e’ from the inlet and walls to ensure full flow development before encountering the particle. The boundary conditions and the domain dimensions ensure the flow field around the particles is free from any boundary effects. An inlet velocity of 0.2 mm/s is initialized in this study. Hence, the Reynolds number (Eq. 1) is quantified as 8, ensuring the flow is in the laminar regime. At low Re, the hydrodynamic forces have a major contribution from the

viscous forces, unlike the turbulent regime. All the particles considered in this study are of the same volume, with an equivalent diameter (the diameter of a sphere with the same volume as that of the particle) of 40 mm.

$$Re = \frac{\rho V d_e}{\mu} \tag{1}$$

Where V is the free stream velocity of water, d_e is the equivalent diameter, ρ is the density of the fluid, and μ is the dynamic viscosity of the fluid (water).

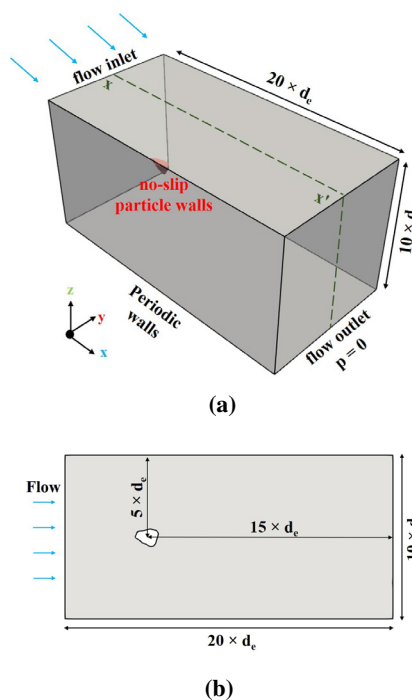
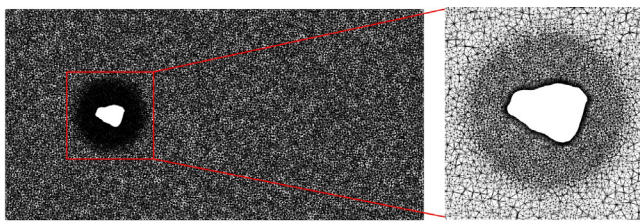


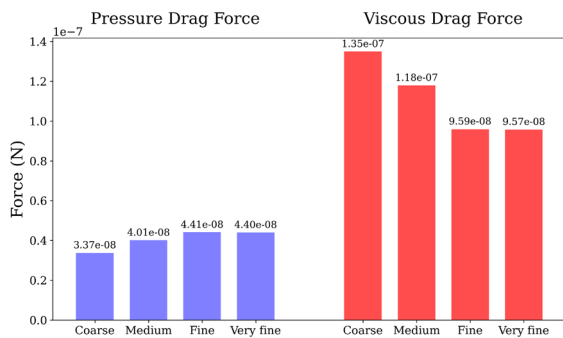
Figure 1: (a). Fluid domain and the boundary conditions, (b). Cross-section (x-x') of the fluid domain (d_e is the diameter of equivalent volume sphere)

*e-mail: rameshkk@iitm.ac.in

OpenFOAM's simpleFoam - steady state solver for incompressible flow [2] is used to simulate the flow around particles. A hybrid TET-HEX meshing approach (Figure 2a) is used for computational efficiency, with a fine boundary layer HEX mesh near particle surfaces to capture near-wall flow phenomena accurately, and a gradually coarsening TET mesh extending to the domain boundaries. The boundary layer mesh uses the inflation technique to mesh 10 layers with a growth rate of 1.1. Mesh independence or sensitivity studies (Figure 2b) were performed to ensure that the adopted mesh resolution was sufficient to capture hydrodynamic behavior without exceeding computational cost.



(a)



(b)

Figure 2: (a). Fluid domain meshing with boundary layer refinement around the particle, (b). Grid convergence study for the elongated particle used in this study

The hydrodynamic forces acting on particles were decomposed into pressure drag and viscous drag components. Pressure drag results from the pressure differential between the upstream and downstream faces of the particle, while viscous drag arises from the shear stresses acting tangentially to the particle surface due to fluid viscosity. These forces were resolved into their X, Y, and Z components to provide an understanding of the forces in the direction of flow and perpendicular to it. The X-component represents the drag force aligned with the flow direction, while the Y and Z components indicate lateral and vertical forces, respectively. The gravitational effects were neglected to isolate the pure hydrodynamic interactions between the fluid and particles without the effect of settling.

The total drag coefficient in the direction parallel to the flow (C_D) for each particle was calculated as the sum of the pressure drag coefficient (PX) and the viscous drag coefficient (VX). Where PX represents the contribution from normal pressure forces and VX accounts for tangential shear stresses. These coefficients are evaluated by inte-

grating the respective forces over the entire particle surface and normalizing by the dynamic pressure and reference area (Eq. 2). The value of C_D depends on the reference area (A_r) chosen, and the projected area of the equivalent volume sphere is considered in this study ($1.26E-3 m^2$). The lateral and vertical hydrodynamic force coefficients are calculated in a similar way [3].

$$C_D = \frac{2F_x}{\rho V^2 A_r} \quad (2)$$

The numerical setup is validated with the empirical drag coefficient of the equivalent sphere given by Eq. 3. The value of C_D obtained from the CFD simulation is 5.09, while that from the empirical relation is 5.142. The error of 1.01% is within acceptable limits. The hydrodynamic lateral and vertical force coefficients of the sphere are 0.

$$(C_D)_{sphere} \approx \frac{24}{Re} + \frac{6}{1 + \sqrt{Re}} + 0.4 \quad (3)$$

Realistic digital representations of the particles were obtained from X-ray CT scanning [4], meshed and imported into the CFD solver for analysis. Three commonly observed particle morphologies - Elongated, Rounded, and Angular are investigated in this study (Figure 3). The morphological characterization of the particles (Table 1) is based on indices that quantify different aspects of the particle form and surface features. Sphericity measures the closeness of a particle to a perfect sphere by comparing the surface area of an equivalent-volume sphere to the actual particle surface area, with values approaching 1.0 indicating more spherical particles. Convexity quantifies the degree of surface irregularities by calculating the ratio of particle volume to its convex hull volume, effectively measuring the presence and extent of concavities.

The Elongation Index (E.I) represents the ratio between the intermediate and major axes of a particle, providing insight into its longitudinal extension, while the Flakiness Index (F.I) compares the minor to intermediate axes, indicating the flatness of the particles. The Corey shape factor (S_f) offers a combined dimensional assessment [1] by incorporating all three principal axes into a single parameter (Eq. 4), with higher values suggesting more equidimensional particles (S_f for a sphere is 1). The surface area to volume ratio provides information about the area of particles, directly influencing fluid-particle interactions. The silhouette area (S_h) represents the maximum projected area of the particle as viewed in the flow direction. These morphological indices collectively provide a comprehensive framework for analyzing particle shape and surficial characteristics [5] to establish correlations with the observed hydrodynamic behavior.

$$S_f = \frac{c}{\sqrt{ab}} \quad (4)$$

Where a , b , and c are the major, intermediate, and minor axes of the particle, respectively.

3 Results and discussions

There is an intricate relationship between shape and surficial parameters with the hydrodynamic behavior in the

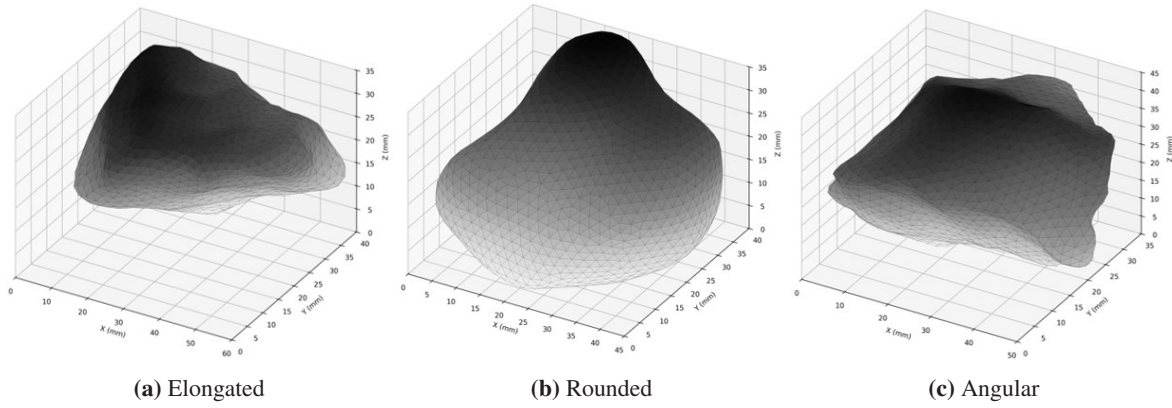


Figure 3: (a). Different particle morphologies considered in this study

Table 1: Particle shape indices

Particle Morphology	Convexity	Sphericity	E.I	F.I	S_f	Surface Area: Volume ratio	S_h : Volume ratio (Major axis)	S_h : Volume ratio (Minor Axis)
Elongated	0.91	0.80	0.98	0.67	0.66	186.52	29.36	61.72
Rounded	0.95	0.91	0.89	0.75	0.70	165.65	29.90	49.25
Angular	0.89	0.82	0.80	0.86	0.77	181.85	32.28	44.15

laminar regime. The hydrodynamic force coefficients of the sphere (with the lowest surface area per given volume and S_f of 1) are chosen as the baseline for comparison. In the orientation with flow parallel to the major axis, the viscous drag always dominated for all particle morphologies due to the higher surface area and the lowest silhouette area. The elongated particles (Figures 4, 5, 6, 7), characterized by a high elongation index (0.98) and the lowest Corey shape factor, demonstrate the most pronounced orientation-dependent hydrodynamic response. On changing the flow direction parallel to the minor axis, a 45.3% increase in total drag was observed compared to the drag force when the flow is parallel to the major axis. The pressure drag coefficients increase from 1.573 when flow aligns with its major axis to 4.578 when flow is parallel to its minor axis (a 191% increase).

Angular particles (Figures 6, 7) characterized by the highest S_f , and the lowest convexity with a higher surface area to volume ratio, is expected to have irregular surface features with a significant viscous drag contribution. Their hydrodynamic signature reveals relatively consistent viscous drag coefficients, showing negligible variation with particle orientation (3.546 for the major axis parallel to the flow and 3.551 for the minor axis parallel to the flow). However, a slight increase in the pressure drag component was observed when the flow is parallel to the minor axis. Rounded particles show intermediate behavior for both the pressure and viscous drag components. Overall, the silhouette area, not the surface area to volume ratio, showed a better trend (inverse variation) for the viscous drag component in the laminar regime, possibly acting as a proxy for the effective wetted area.

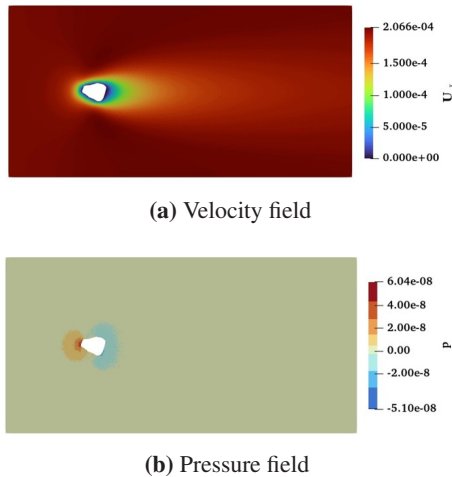


Figure 4: Velocity and pressure around Elongated particle (oriented with major axis parallel to the flow direction)

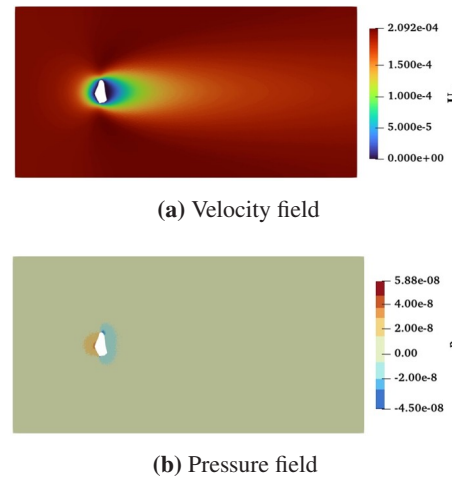


Figure 5: Velocity and pressure around Elongated particle (oriented with minor axis parallel to the flow direction)

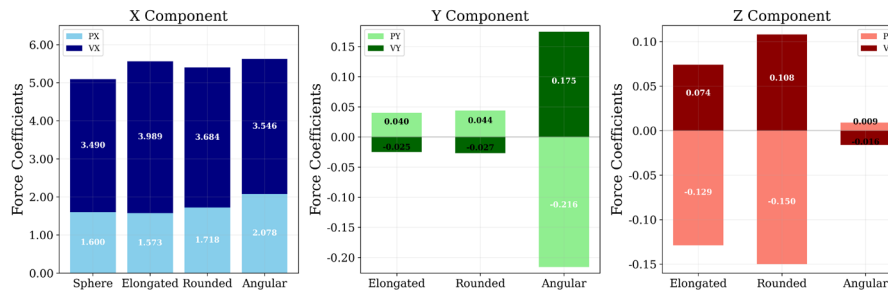


Figure 6: Hydrodynamic force coefficients for flow parallel to the major axis of the particles

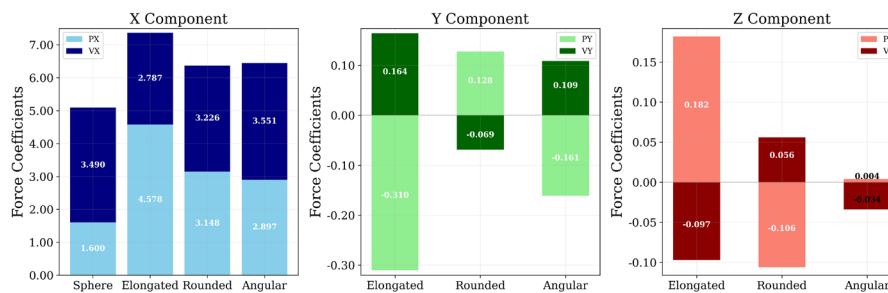


Figure 7: Hydrodynamic force coefficients for flow parallel to the minor axis of the particles

4 Conclusions

The influence of particle morphology on the hydrodynamic behavior was investigated in the laminar regime. Particle shape characteristics influence both the magnitude and directional distribution of hydrodynamic forces. The S_f emerges as the most reliable morphological predictor for hydrodynamic behavior across different flow orientations. Particles with higher S_f (closer to unity, indicating more equidimensional geometry) exhibit significantly more consistent hydrodynamic responses regardless of flow direction. This finding is exemplified by the angular particle ($S_f = 0.77$), which showed minimal variation in viscous drag coefficients between major and minor axis orientations (3.546 vs 3.551), contrasting sharply with the elongated particle ($S_f = 0.66$) that demonstrated a 45.3% increase in total drag when flow orientation changed from major to minor axis.

Lower S_f correspond to greater anisotropy in the hydrodynamic response, as evidenced by the increase in pressure drag coefficient 191% of the elongated particle when the flow transitioned from parallel to the major axis (1.573) to parallel to the minor axis (4.578). The orientation sensitivity diminishes as the S_f approaches unity, suggesting that more equidimensional particles provide more consistent hydrodynamic behavior with different orientations. However, local surficial features also play a role in pressure distribution and flow field around the particle, thus deviating from the perfect relation of the pressure drag with S_f . In the laminar regime, the viscous component of the drag force shows an inverse variation with the silhouette area. Negative lateral forces indicate that the net hydrodynamic force is acting in the negative direction of the Y

or Z axes, pushing the particle sideways or downward relative to the coordinate system. These forces arise from flow asymmetries around irregularly shaped particles that create unbalanced pressure distributions, with the magnitude and direction varying depending on particle orientation and surface irregularities.

A detailed study on the sensitivity of force coefficients to varying Re would give a better understanding of the influence of particle morphology and surface features on the hydrodynamic response.

References

- [1] Deal, E., Venditti, J.G., and Perron, J.T. Grain shape effects in bed load sediment transport. *Nature* **613**, 298-302 (2023). <https://doi.org/10.1038/s41586-022-05564-6>
- [2] OpenFOAM Foundation. OpenFOAM: The Open Source CFD Toolbox, 2023.
- [3] Qi, J., Fei, W., Narsilio, G.A. An LBM study on the local fluid flow in irregular monodisperse granular assemblies from DEM: Effects of particle shape. *Computers and Geotechnics* **177**, 106817 (2025). <https://doi.org/10.1016/j.compgeo.2024.106817>
- [4] Kalyan, N.S.S.P., Fukumoto, Y., Kandasami, R.K. Investigating rock particle breakage using 3D coupled peridynamics-discrete element method: Emphasis on local surface features. *Engineering Fracture Mechanics* **312**, 110585 (2024). <https://doi.org/10.1016/j.engfracmech.2024.110585>
- [5] Á. Vergara, and D. Wei, “Drag coefficient for irregularly shaped grains: rotational dependence at various Reynolds numbers,” *J. Fluid Mech.*, vol. 994, A1, 2024. <https://doi.org/10.1017/jfm.2024.562>